Field-Theoretic Simulations of Bottlebrush Copolymers

Russell K. W. Spencer* and Mark W. Matsen†

Department of Chemical Engineering,

Department of Physics & Astronomy,

and Waterloo Institute for Nanotechnology,

University of Waterloo, Waterloo, Ontario N2L 3G1, Canada

(Dated: October 4, 2018)

Abstract

Traditional particle-based simulations struggle with large bottlebrush copolymers, consisting of many side chains grafted to a backbone. Field-theoretical simulations (FTS) allow us to overcome the computational demands in order to calculate their equilibrium behavior. We consider bottlebrushes where all grafts are symmetric diblock copolymers, focusing on the order-disorder transition (ODT) and the size of ordered domains. Increasing the number of grafts and decreasing the spacing between them both raise the transition temperature. The ODT and lamellar period asymptotically approach constants as the number of grafts increases. As the spacing between grafts becomes large, the bottlebrushes behave like diblock copolymers, and as it becomes small, they behave like starblock copolymers. In between, the period increases, reaching a maximum when the spacing is approximately 0.35 times the length of the grafts. Comparison of FTS with mean-field calculations allows us to assess the effect of compositional fluctuations. Fluctuations suppress ordering, while having little effect on the period, as is the case for diblock copolymers.

I. INTRODUCTION

Bottlebrush copolymers are a new and exciting class of materials. They consist of many (typically 10-100) side chains grafted along a backbone. This leads to ultrahigh molecular weights and new behaviors, specific to bottlebrushes. These include larger domains than those of linear molecules,[1–3] increasing the range of applications. There is also less entanglement, leading to faster dynamics and improved ordering, as compared with linear molecules. The large number of grafts enhances domain-bridging, leading to the improvement of mechanical properties. For these reasons, they are ideal candidates for a range of advanced materials and applications,[4–8] for example, surface coatings,[9] photonic crystals,[3,10–12] lithography[13] and thermoplastic elastomers.[14–16]

The reduction in entanglement is partly attributed to large persistence lengths resulting from the dense packing of grafts. Steric repulsion causes grafts to stretch, but also impedes backbone bending.[8,17,18] Measurements of bottlebrushes in solution have found backbone persistence lengths of up to an order of magnitude larger than that of the bare backbone.[5] Quantitative modeling[19] of melts of bottlebrushes, however, has found that the backbone remains quite flexible, not at all rod-like, as assumed in some studies.[3,20,21] They deduced the persistence length by modeling the backbone as a worm-like chain, and adjusting the rigidity to match the experiments.[19]

One interesting bottlebrush architecture involves using symmetric diblock copolymers as grafts. There has been a growing effort to synthesize and characterize such polymers experimentally,[14–16] and their equilibrium phase behavior has recently been examined. The experiments have found that the bottlebrushes spontaneously form lamellae with exceptionally high degrees of long-range order. They also found that unless the number of side chains, M, is small, the order-disorder transmission (T_{ODT}) is independent of M and close to that reported for simple diblock copolymer melts. The resulting materials were found to be exceptional thermoplastic elastomers, likely due to the high degree of domain bridging among the connected grafts.

Traditional, particle-based, simulation methods are not easily amenable to bottlebrushes, because of huge computational demands due to the immense size of these molecules. To overcome this requires unrealistic simplifications of the molecular architecture.[22] Field-based techniques, on the other hand, are highly efficient for large molecules and can take advantage

of molecular symmetries to further increase efficiency.[19] Nevertheless, there are challenges for field-theoretic simulations (FTS). Backbone rigidity provides the biggest challenge, as FTS of worm-like chains are very computational. The increased rigidity, however, is only significant if the grafts are densely-packed,[23] and simulating the backbone as flexible may be sufficient.

In this work, we use Monte Carlo field-theoretic simulations (MC-FTS) to examine the equilibrium behavior of melts of bottlebrushes with symmetric diblock copolymer grafts. We examine the effect of changing the number of grafts and the space between them. Specifically, we present results for the order-disorder transition and the lamellar periods. The MC-FTS are also compared with mean-field calculations in order to gauge the effect of compositional fluctuations.

II. THEORY AND SIMULATION

This work examines a melt of n bottlebrush copolymers with M AB diblock copolymers grafted by their B ends regular intervals along a backbone (see Fig. 1). The grafts each contain N segments, a fraction f of which are A type, and the backbone contains αN segments between grafts (i.e. a total of $(M-1)\alpha N$ segments). The molecules are modeled as flexible Gaussian chains, where each segment has a statistical length, a. Thus the natural end-to-end length of a graft is $R_0 = a\sqrt{N}$, which we use as our unit length. We assume a fixed volume of ρ_0^{-1} for the graft segments and ignore the volume of the backbone. Thus, the melt is incompressible with a fixed volume of $V = nMN/\rho_0$. Furthermore, we only consider interactions between the A and B segments of the grafts, which are controlled by the usual Flory-Huggins parameter, χ. Fluctuations are controlled by the concentration of grafts, $nM/V = \sqrt{\bar{N}}/R_0^3$, where $\bar{N} = a^6\rho_0^2 N$ is the invariant polymerization index of a graft.

Neglecting the volume of the backbone and its interactions has the benefit of reducing the number of system parameters. Equally important, it reduces the system to two components (i.e. A and B), which simplifies the FTS.[24] Naturally, the volume of the backbone can be ignored when α is small. Furthermore, when the grafts are densely packed, the A blocks will be excluded from contacting the backbone. As such, the interaction energy of the backbone will be relatively constant and therefore can be ignored.[19] Although these approximations are only valid for small α, we do nevertheless examine the model over the entire range of α.

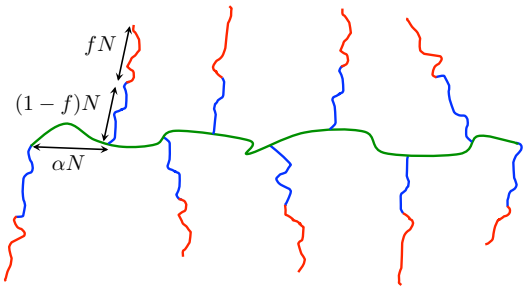


FIG. 1: Illustration of a bottlebrush with $M = 9$ diblock copolymer grafts, each with fN A segments and $(1-f)N$ B segments. The grafts are separated by αN segments.

A. Field-Theoretic Hamiltonian

In field-theoretic simulations, the Hamiltonian for a two-component melt,

$$\frac{H[W_-, W_+]}{nMk_BT} = \frac{1}{M}\ln\left(\frac{V}{Q}\right) + \frac{1}{V}\int\left(\frac{W_-^2}{\chi_b N} - W_+\right)d\mathbf{r}, \tag{1}$$

depends on the fields $W_-(\mathbf{r})$ and $W_+(\mathbf{r})$, which act on the difference, $\hat{\phi}_-(\mathbf{r}) = \hat{\phi}_A(\mathbf{r}) - \hat{\phi}_B(\mathbf{r})$, and sum, $\hat{\phi}_+(\mathbf{r}) = \hat{\phi}_A(\mathbf{r}) + \hat{\phi}_B(\mathbf{r})$, of the instantaneous concentrations of A and B segments, respectively. The function $Q[W_-, W_+]$ is the partition function a single bottlebrush in the fields. Note that the bare χ_b will eventually be replaced by an effective χ.

In order to calculate Q, we need to determine partial partition functions, or propagators, for different parts of the bottlebrush. The "forward" propagator, $q(\mathbf{r}, s)$, for a graft is the partition function for the free end of a graft, with the sN'th segment fixed at $\mathbf{r}$. It satisfies

$$\frac{\partial q}{\partial s} = \left[\frac{R_0^2}{6}\nabla^2 + \frac{1}{2}(W_- \pm W_+)\right]q, \tag{2}$$

with "+" for $0 < s < f$ and "−" for $f < s < 1$. Equation (2) is solved using a fourth-order pseudospectral algorithm,[25] with the initial condition $q(\mathbf{r}, 0) = 1$. The partition function for an entire graft with its grafted end at $\mathbf{r}$ is $q(\mathbf{r}, 1)$.

We parameterize the backbone by s, which runs from $s = 0$ to $(M-1)\alpha$, and calculate its propagator, $q_b(\mathbf{r}, s)$. Between the grafts, the propagator satisfies

$$\frac{\partial q_b}{\partial s} = \frac{R_0^2}{6}\nabla^2 q_b. \tag{3}$$

Due to the attachment of grafts, $q_b(\mathbf{r}, s)$ is discontinuous at $s = s_i \equiv (i-1)\alpha$, where $i = 1, 2, ..., M$. To distinguish the two sides of the discontinuities, we denote the value of the backbone parameter before and after the discontinuities as s_i^- and s_i^+ respectively. Using this notation, the discontinuities are given by

$$q_b(\mathbf{r}, s_i^+) = q_b(\mathbf{r}, s_i^-) q(\mathbf{r}, 1). \tag{4}$$

The backbone propagator is solved starting from the initial condition $q_b(\mathbf{r}, 0^-) = 1$. The partition function for an entire bottlebrush is then given by

$$Q[W_-, W_+] = \int q_b(\mathbf{r}, s_M^+) d\mathbf{r}. \tag{5}$$

B. Field-Theoretic Simulations

Monte Carlo field-theoretic simulations (MC-FTS) are based on techniques more fully described in previous work.[26,27] The statistical mechanics of the field-based model entails performing functional integrals over the fields, $W_-(\mathbf{r})$ and $W_+(\mathbf{r})$, to evaluate the partition function

$$Z \sim \int \exp\left(-\frac{H[W_-, W_+]}{k_B T}\right) \mathcal{D}W_- \mathcal{D}W_+. \tag{6}$$

Employing standard Monte Carlo techniques is complicated, because $W_+(\mathbf{r})$ takes on imaginary values. This problem can be avoided by simulating only $W_-(\mathbf{r})$ and setting $W_+(\mathbf{r})$ to its saddle point, $w_+(\mathbf{r})$. This enforces incompressibility in a mean-field manner,

$$\phi_+(\mathbf{r}) \equiv \phi_A(\mathbf{r}) + \phi_B(\mathbf{r}) = 1, \tag{7}$$

where $\phi_A(\mathbf{r})$ and $\phi_B(\mathbf{r})$ are average A and B concentrations in the system of non-interacting molecules. For each $W_-(\mathbf{r})$, we adjust $w_+(\mathbf{r})$ iteratively using Anderson mixing[28] until

$$\left[\frac{1}{V}\int (\phi_+(\mathbf{r}) - 1)^2 d\mathbf{r}\right]^{1/2} < \varepsilon. \tag{8}$$

A tolerance of $\varepsilon = 10^{-4}$ is sufficient for our calculations.

Finding $\phi_A(\mathbf{r})$ and $\phi_B(\mathbf{r})$ requires us to calculate the "back" propagator for the grafts, $q^\dagger(\mathbf{r}, s)$, which satisfies Eq. (2), with one side multiplied by -1. We can propagate backwards along all grafts at once from

$$q^\dagger(\mathbf{r}, 1) = \sum_{i=1}^{M} q_b(\mathbf{r}, s_i^-) q_b(\mathbf{r}, s_{M+1-i}^-), \tag{9}$$

which is the sum of the initial conditions for each individual graft. In this way, the concentrations from all of the grafts are given by the simple expressions,

$$\phi_A(\mathbf{r}) = \frac{V}{Q}\int_0^f q(\mathbf{r},s)q^\dagger(\mathbf{r},s)ds, \tag{10}$$

$$\phi_B(\mathbf{r}) = \frac{V}{Q}\int_f^1 q(\mathbf{r},s)q^\dagger(\mathbf{r},s)ds. \tag{11}$$

Implementation of the saddle-point approximation for $W_+(\mathbf{r})$, reduces Eq. (6), to

$$Z \sim \int \exp\left(-\frac{H[W_-,w_+]}{k_BT}\right)\mathcal{D}W_-. \tag{12}$$

The fields $W_-(\mathbf{r})$ and $w_+(\mathbf{r})$, and thus the Hamiltonian, $H[W_-,w_+]$, are real, rendering the system amenable to standard Monte Carlo techniques. Each Monte Carlo (MC) step involves making a small change, or "move," to the system, followed the recalculation of $w_+(\mathbf{r})$, the evaluation of $H[W_-,w_+]$ and the application of the standard Metropolis MC criteria to accept or reject the move.

For changes in $W_-(\mathbf{r})$, we alternate between a real-space move, where the change in $W_-(\mathbf{r})$ at each point, $\mathbf{r}$, is selected from a uniform distribution, and a Fourier-space move, where the change in $W_-(\mathbf{k})$ at each wavevector, $\mathbf{k}$, is selected from a uniform distribution weighted by the Fredrickson-Helfand structure function for diblock copolymers, $S_{\rm FH}(k)$.[29] The amplitude of each move is adjusted during the initial part of the equilibration period, to achieve an acceptance probability of $\sim 40\%$. In some simulations of the lamellar phase, we also employ a "box move" to equilibrate the lamellar period.[30] This is done by varying the box dimension perpendicular to the lamellae, L_x, with the parallel dimensions following $L_y = L_z = \sqrt{V/L_x}$ so as to maintain constant volume, V.

C. Ultraviolet Divergence

The fields $W_-(\mathbf{r})$ and $w_+(\mathbf{r})$ are represented on discrete, three-dimensional grids with m_γ points spaced by Δ_γ in the γ-dimension, giving box lengths of $L_\gamma = m_\gamma\Delta_\gamma$. Our simulation boxes are typically cubic, but deviate therefrom when employing the box move. In these cases, lengths are altered by changing the grid spacing, leaving m_γ fixed.

One might expect that decreasing the grid spacing, Δ_γ, would lead to more accurate simulations, and that the result would converge as $\Delta_\gamma \to 0$. However, it actually leads to a diverging contribution to the free energy, which acts to disorder the melt. This ultraviolet

(UV) divergence has been thoroughly discussed in previous work.[30,31] Fortunately, the diverging part of the free energy can be absorbed into the bare interaction parameter, χ_b, of the Hamiltonian, resulting in a renormalized or "effective" χ, given by

$$\frac{\chi}{\chi_b} = 1 - \frac{12R_0}{\pi^3\sqrt{\bar{N}}}\int_0^{\Lambda_z}\int_0^{\Lambda_y}\int_0^{\Lambda_x}\frac{dk_x dk_y dk_z}{k_x^2+k_y^2+k_z^2}, \tag{13}$$

where $\Lambda_\gamma = \pi/\Delta_\gamma$ is the wavevector cutoff.[32] We typically use the same grid spacing in each direction, $\Delta_\gamma = \Delta$, which simplifies Eq. (13) to[27]

$$\frac{\chi}{\chi_b} = 1 - \frac{2.333}{\sqrt{\bar{N}}}\frac{R_0}{\Delta}. \tag{14}$$

In each of our simulations, we set $m_\gamma = 16$ and $L_\gamma = 2D$, where D is the equilibrium lamellar period. Previous studies have shown that eight points per lamellar period is sufficient to obtain Δ-independent behavior[27,30] and that two periods is sufficient to eliminate significant finite-size effects.[33] Since D varies with model parameters, so does Δ and thus χ/χ_b. This ratio also changes in the box move, and therefore we adjust χ_b, according to Eq. (13), in order to maintain the same χ throughout the simulation.

D. Parallel Tempering

The order-disorder transition (ODT) is located using parallel tempering (PT), which involves conducting a set of simulations at closely-spaced χN values, spanning the ODT.[27,34] After each replica has evolved for a number of MC steps (we use 10^3) "swap" moves are attempted, where configurations at adjacent χN values can be exchanged. The acceptance of these moves is subject to the usual MC criteria. This allows for faster equilibration, particularly for the purpose of annealing out defects in the ordered phase.

To locate the ODT from PT simulations, we define an order parameter, which is small in the disordered (DIS) and large in the lamellar (LAM) phase. Our order parameter, $\langle\Psi\rangle$, is defined as the ensemble average of[27]

$$\Psi = V^{-2}\max_{\mathbf{k}}[W_-(\mathbf{k})W_-(-\mathbf{k})]. \tag{15}$$

Two sets of PT simulations are conducted, one starting from DIS and the other from LAM. The result is a pair of $\langle\Psi\rangle$ vs. χN curves, which generally reveals an interval over which both phases persist for the duration of the simulation. This metastability interval brackets the ODT.

We also tried locating the ODT using thermodynamic integration,[33,35,36] however, PT turned out to be more efficient. The weakly first-order nature of the ODT leads to easy transitions between LAM and DIS, allowing PT to precisely locate the transition. It also leads to small differences in the slopes of free energy vs. χN curves, and thus imprecision in the ODT determined by TI. TI is more useful for more strongly first-order transitions and larger simulation volumes.

E. Mean-Field Calculations

SCFT involves solving Eq. (6) using the saddle-point approximation for both the $W_+(\mathbf{r})$ and $W_-(\mathbf{r})$ fields. The saddle-point $w_+(\mathbf{r})$ is evaluated as before, in section II B. The other saddle-point $w_-(\mathbf{r})$ is evaluated similarly, and satisfies

$$w_-(\mathbf{r}) = -\frac{1}{2}\chi N \phi_-(\mathbf{r}), \tag{16}$$

where $\phi_-(\mathbf{r}) \equiv \phi_A(\mathbf{r}) - \phi_B(\mathbf{r})$.

We also employ the random phase approximation (RPA),[37–39] in which the partition function for a block copolymer with an arbitrary number of blocks, and no loops, is approximated as

$$\frac{Q}{V} \approx 1 + \frac{1}{2(2\pi)^3 V} \int \sum_{i,j} S_{ij}(\mathbf{k}) w_i(-\mathbf{k}) w_j(\mathbf{k}) d\mathbf{k}, \tag{17}$$

where $w_i(\mathbf{k})$ is the field in Fourier space acting on the segments in block i. The function

$$S_{ij} = \begin{cases} g(x, f_i), & i = j \\ h(x, f_i) h(x, f_j) \exp(-x \Delta s_{ij}), & i \neq j \end{cases} \tag{18}$$

corresponds to an interaction between blocks i and j, where $g(x,s) \equiv 2[\exp(-sx) + sx - 1]/x^2$ and $h(x,s) \equiv [1 - \exp(-sx)]/x$ are Debye and Debye-like functions, respectively, $f_i \equiv N_i/N$ is the polymerization of the i'th block relative to the reference polymerization N, Δs_{ij} is the distance along the polymer that separates i and j, and $x \equiv k^2 R_0^2/6$.

For polymers with only A and B segments, we separate the terms in the sum into AA,

BB and AB interaction terms, whereby Eq. (17) reduces to

$$\frac{Q}{V} \approx 1 \; + \; \frac{M}{2(2\pi)^3 V} \int [S_{AA} w_A(-\mathbf{k}) w_A(\mathbf{k}) + \; S_{BB} w_B(-\mathbf{k}) w_B(\mathbf{k}) + 2 S_{AB} w_A(-\mathbf{k}) w_B(\mathbf{k})] d\mathbf{k}. \tag{19}$$

For bottlebrushes with diblock copolymer grafts,

$$\begin{aligned} S_{AA} &= g(x,f) + \mathcal{A} h^2(x,f) \exp(-2x(1-f)), \\ S_{BB} &= g(x,1-f) + \mathcal{A} h^2(x,1-f), \\ S_{AB} &= h(x,f) h(x,1-f) \left(1 + \mathcal{A} \exp(-x(1-f)\right). \end{aligned} \tag{20}$$

The quantity

$$\mathcal{A} = \frac{1}{M} \sum_i \sum_{j \neq i} \exp(-x|i-j|\alpha) \tag{21}$$

accounts for the separation of the grafts along the backbone. It can be accurately approximated in various limits. For $\alpha \to 0$, it reduces to $\mathcal{A} = M - 1$, which corresponds to starblock copolymers,[40] and for $\alpha \to \infty$ or $M = 1$, it becomes $\mathcal{A} = 0$ which corresponds to diblock copolymers.[37] In the case of large M, $\mathcal{A} \approx 2/(e^{\alpha x} - 1)$ From this approximation of Q/V, the evaluation of the lamellar period, $D = 2\pi/k^*$, and the order-disorder transition, $(\chi N)_{ODT}$, follows.[39]

III. RESULTS

This work examines a melt of bottlebrush copolymers, where each graft is a diblock copolymer. The grafts are symmetric (i.e., $f = 1/2$) and have an invariant polymerization index of $\bar{N} = 10^4$. Melts are contained in boxes, typically cubic, with periodic boundary conditions, represented using $m_\gamma = 16$ points in each direction. The box dimensions, $L_\gamma = L$, are typically equal and chosen to accommodate two lamellar periods.

The order-disorder transition (ODT) is located using parallel tempering (PT). Two separate PT simulations are performed, one from the disordered (DIS) phase and the other from the lamellar (LAM) phase, producing a metastability interval bracketing the ODT. An example is shown in Fig. 2. We locate the ODT in three steps. An initial pair of PT simulations gives us an approximate location for the ODT. This is followed by a box-move

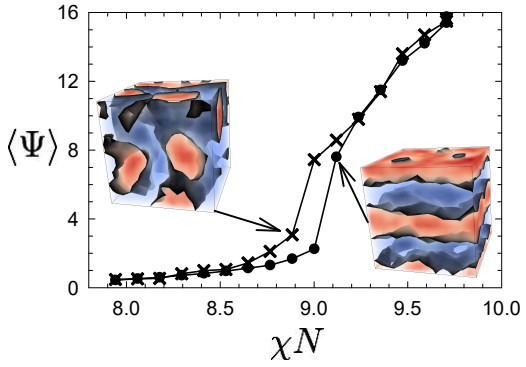


FIG. 2: Order parameter for a $M = 9$ bottlebrush with $\alpha = 0.1$ obtained from a pair of parallel tempering runs, one starting from DIS (circles) and another starting from LAM (crosses). The metastability loop brackets the ODT, i.e., $8.9 < (\chi N)_{ODT} < 9.1$. The inset shows snapshots of $W_{-}(\mathbf{r})$ for small (i.e. DIS) and large (i.e. LAM) order parameters.

simulation to correct the lamellar period. Finally, we determine the ODT at the corrected period from a second pair of PT simulations.

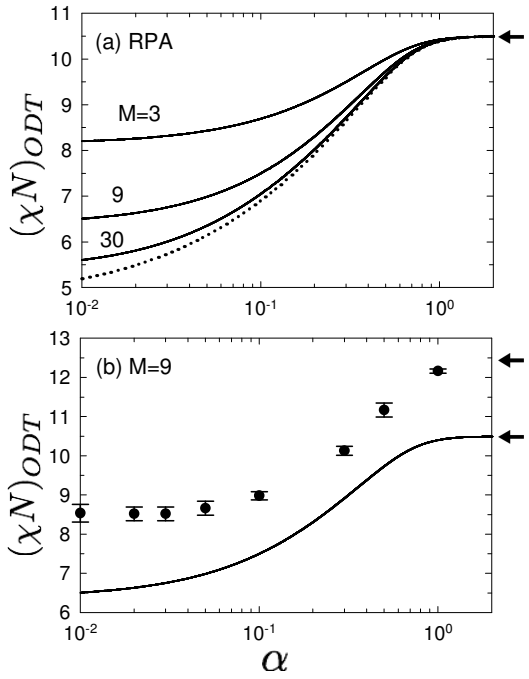


FIG. 3: (a) ODT as a function of α, calculated for different M using RPA. The $M \to \infty$ limit is denoted with a dotted curve. (b) Comparison of the FTS ODT (symbols) with the RPA ODT (curve) for $M = 9$. The $\alpha \to \infty$ limits are indicated by arrows.

Figure 3(a) shows the RPA (or mean-field) prediction for the ODT as a function of spacing between grafts (i.e. α) for different numbers of grafts, M. The $\alpha = 0$ limit corresponds to starblocks,[41] for which the ODT decreases as the number of grafts, M, is increased. As α increases, the ODTs increase monotonically to a common $\alpha \to \infty$ limit, which corresponds to the simple diblock copolymer melt (i.e., $(\chi N)_{ODT} = 10.495$). In reality, our assumptions become inaccurate for large α as the volume of the backbone becomes significant. A more complete calculation would need to consider the volume of the backbone and its interactions with the grafts.

The FTS prediction of the ODT is compared to RPA for $M = 9$ bottlebrushes in Fig. 3(b). The error bars denote the width of the metastability interval (see Fig. 2). The dependence on α is qualitatively the same, but fluctuations shift the FTS ODTs to larger $(\chi N)_{ODT}$. The magnitude of the shift is about 2 units over the whole range of α. This is similar to the shift of 2.6 predicted for simple diblock copolymer melts of $\bar{N} = 10^4$.[42]

Our result that the ODT of bottlebrushes asymptotically approaches a constant as grafting density increases (α decreases) is qualitatively consistent with experiments.[16] They find that the ODT does not change when the grafting density is increased beyond α of a few percent, below which we find that the bottlebrush is already close to the starblock limit and decreasing it further has little effect on the ODT. This is particularly true in the simulation results. The ODT found in experiments, however, approaches that of a diblock, not a starblock copolymer. It is not clear why this is the case.

For low grafting densities, experiments find that decreasing the grafting density suppresses ordering.[16] This is qualitatively consistent with our result; however, they did not find that the ODT approaches that of a diblock copolymer. It is not surprising that there would be disagreement for low grafting densities because our model ignores the backbone volume and its interactions with grafts.

Figure 4(a) shows the lamellar period at the ODT as calculated by RPA. Interestingly, the period does not vary monotonically between the starblock ($\alpha \to 0$) and diblock ($\alpha \to \infty$) limits. The maximum period occurs at $\alpha \approx 0.35$ almost independently of M. This trend is also present in the FTS as seen in Fig. 4(b) for $M = 9$. The larger periods predicted by FTS relative to RPA can be attribured to the shift in $(\chi N)_{ODT}$. To illustrate this, we also plot the SCFT prediction of D (crosses) calculated at the $(\chi N)_{ODT}$ of the FTS. The accurate match in D, when evaluated at equal values of χN, is consistent with the previous finding[43]

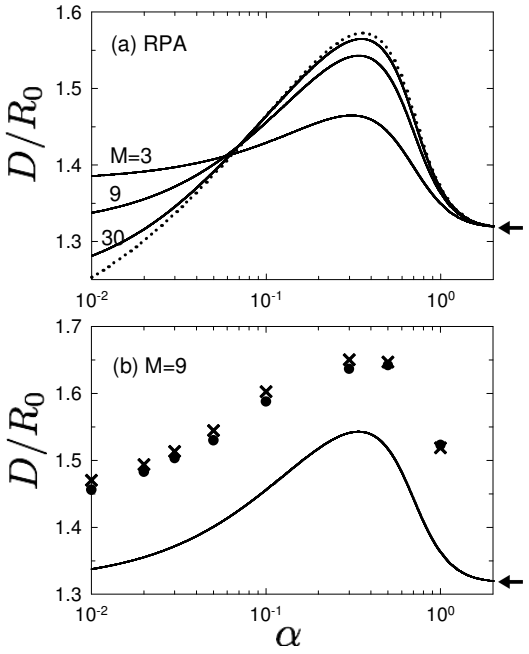


FIG. 4: (a) Lamellar period at the ODT as a function of α calculated for different M using RPA. The $M \to \infty$ limit is denoted with a dotted curve. (b) Comparison of the FTS period (circles) and SCFT period (crosses) with the RPA period (curve) for $M = 9$. Note that the SCFT period is evaluated at the FTS ODT. The $\alpha \to \infty$ limits are indicated by arrows.

that mean-field theory treats ordered phases accurately.

We next turn our attention to the effect of increasing the number of grafts, M, on the ODT, illustrated in Fig. 5. As M increases, the ODT asymptotically approaches the limit discussed in section II E. Increasing the number of grafts past $M \approx 30$ does not significantly change the ODT. A finite limit is approached even for starblocks ($\alpha = 0$) for which all grafts are attached to the same point and graft-graft correlations do not decay. The approach, however, is slower than for any of the finite-α bottlebrushes considered. The dependence of the ODT determined by FTS is qualitatively the same as that predicted by RPA, but is, once again, shifted to higher χN by approximately 2 units over the entire range.

The lamellar period, illustrated in Fig. 6, approaches the $M \to \infty$ limit and does not change considerably past $M \approx 30$. For small numbers of grafts, the period always increases with M, which leads to non-monotonic behavior in D vs. M when the $M \to \infty$ period is below that of the diblock ($M = 1$). Once again, mean-field theory (RPA) appears to underestimate the lamellar period at the ODT, however, this can be attributed to the difference

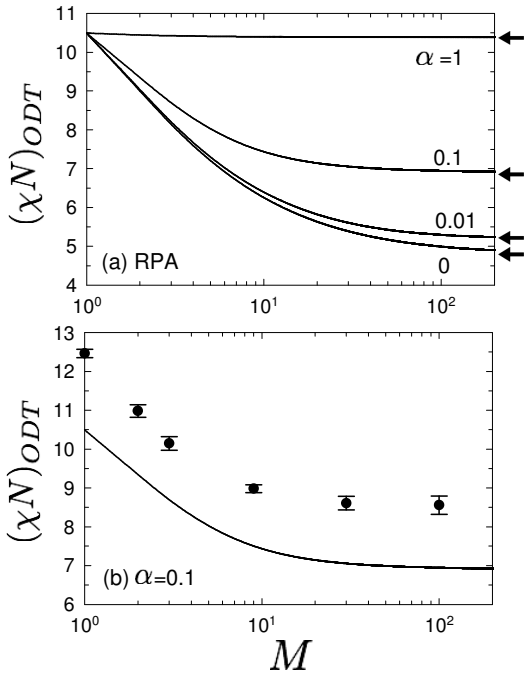


FIG. 5: (a) ODT as a function of M, calculated for different α using RPA. The $M \to \infty$ limits are indicated by arrows. (b) Comparison of the FTS ODT (symbols) with the RPA ODT (curve) for $\alpha = 0.1$.

in the ODT found from mean-field theory and FTS. This is evident by the agreement in Fig. 6(b) between FTS and SCFT conducted at the same χN.

IV. DISCUSSION

Field-theoretic simulations have allowed us to simulate large bottlebrushes with many grafts. Using our algorithm, the computationally intensive part of the simulations are independent of the number of grafts, M. This is because all of the grafts are identical, allowing their concentrations to be evaluated simultaneously. There was a small dependence of total computation time on M because the number of Anderson mixing steps required to find $w_+(\mathbf{r})$ increased gradually for larger M.

We ignored the volume and interactions of the backbone, in order to simplify the model and thus reduce the number of system parameters. Nevertheless, including these features is, in principle, straightforward.[24] It would involve calculating the concentration of the backbone, $\phi_C(\mathbf{r})$, and two new interaction parameters χ_{AC} and χ_{BC}. The field-theoretic Hamil-

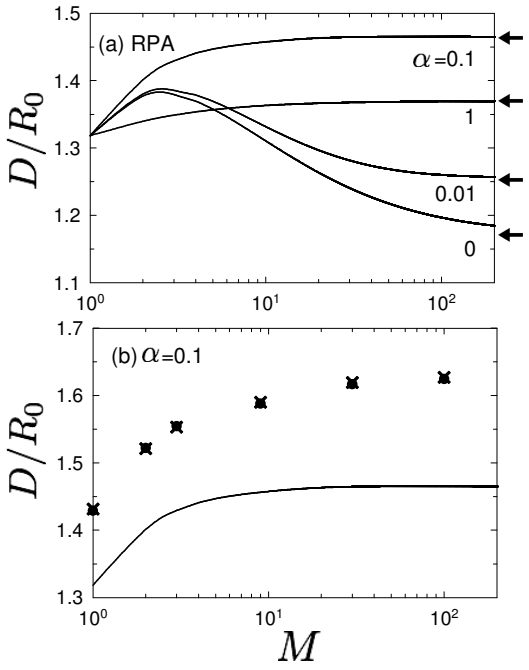


FIG. 6: (a) Lamellar period at the ODT as a function of M calculated for different α using RPA. The $M \to \infty$ limits are indicated with arrows. (b) Comparison of the FTS period (circles) and SCFT period (crosses) with the RPA period (curve) for $\alpha = 0.1$. Note that the SCFT period is evaluated at the FTS ODT.

tonian would also include one new field, which could be real or imaginary depending on the χ parameters. If real, then it would simply be a matter of simulating two fluctuating fields instead of one. If, on the other hand, it is imaginary, we would have to apply the saddle-point approximation as we did for $W_+(\mathbf{r})$, to obtain a real-valued Hamiltonian. The mean-field treatment of $W_+(\mathbf{r})$ has proven to be reasonably accurate,[26,44] and one would hope the same is true for the additional field.

The invariant polymerization index of the grafts was set to a value $\bar{N} = 10^4$, which is somewhat larger than typical of experiments.[16] This was done in order to account for the UV divergence using the effective χ defined in Eq. (13). For smaller $\bar{N}$, this renormalization begins to fail, in that the results do not converge as $\Delta \to 0$. An alternative definition of χ was proposed, which appeared to work for diblock copolymers,[30] but failed when applied to homopolymer blends.[31] Any legitimate definition needs to work for all architectures, and so the problem is still unresolved. However, we are currently investigating a promissing non-linear definition[45] akin to the effective χ defined by Morse and coworkers for particle-based

simulations.[42,46]

For the current bottlebrush architecture, the tension in the backbone should be modest, allowing us to use the Gaussian chain model. Other situations, such as diblock brushes with A homopolymer grafts at one end and B homopolymer grafts at the other, may result in much higher tensions.[19] To prevent overstretching, previous SCFT calculations have modeled the backbone as a worm-like chain.[19] This is unfeasible in FTS, due to the high computational cost. Another approach is to use the freely-jointed chain with bonds of fixed length, which can be done at little computational cost through a simple modification of Eq. (3).[47]

One limitation of our MC-FTS procedure is that the saddle-point approximation for $W_+(\mathbf{r})$ does not treat incompressibility properly and thus ignores certain steric effects. In real bottlebrushes, excluded volume interactions between the densely-packed grafts lead to stretching of the grafts (i.e. bottlebrush-like conformations). This crowding of the grafts also inhibits bending of the backbone, leading to backbone stiffening. Although we expect such effects to be small,[19] they are required for a more complete description of bottlebrushes.

Without the saddle-point approximation, the Hamiltonian, and thus Boltzmann weight, are complex-valued making normal statistical mechanics inapplicable. One way around this is to use complex Langevin field-theoretic simulations (CL-FTS).[48–50] They will also experience the same UV divergence discussed in section II C. This is a general consequence of point-like interactions between thread-like polymers with rigorously-enforced incompressibility in the standard Gaussian chain model.[51] Fredrickson and coworkers deal with it by altering the model, specifically, smearing the interactions and concentrations and introducing compressibility.[36] Although this removes the UV divergence, it is still necessary to define an effective χ, in order to relate the results to those of the standard Gaussian chain model. In an effort to do so, they define χ so as to match the spinodal of the diblock copolymer melt from their model to that of the standard Gaussian chain model. They suggested that a superior approach would be the Morse calibration procedure[42,46] mentioned above.

The steps taken to remove the UV divergence can potentially negate the steric effects, if the smearing or compressibility is too great. For instance, the range of the smearing must be less than the spacing between grafts. It is unclear how much compressibility can be tolerated, but too much will allow the chains to simply overlap. The removal of the UV divergence does not, in principle, require large degrees of smearing or compressibility, but the feasibility of the simulation may. The CL-FTS are known to produce unstable trajectories if

the compressibility is too low, particularly at experimentally relevant values of $\bar{N}$.[50,52] Thus it remains unclear if CL-FTS could in fact account for subtle steric effects of the bottlebrush architecture.

V. SUMMARY

Field-theoretic simulations (FTS) were used to examine the equilibrium behavior of bottlebrushes with M symmetric diblock copolymer grafts of polymerization N spaced by αN along the backbone. The backbone and grafts were both modeled as flexible Gaussian chains. To simplify the calculation, the volume of the backbone and its interactions with the grafts were ignored. The invariant polymerization index of the grafts, which controls the strength of fluctuations, was set to $\bar{N} = a^6\rho_0^2 N = 10^4$. To assess fluctuation effects, our FTS were directly compared to mean-field theory.

At the high invariant polymerization index of our calculations, fluctuation effects were relatively small and thus our FTS agreed qualitatively with mean-field theory. As the number of grafts increased, for a fixed spacing, the order-disorder transition and lamellar period approached a constant, and having more than $M \approx 30$ grafts did not substantially change the equilibrium behavior. Increasing the space between grafts, α, caused the bottlebrush to behave like a diblock copolymer, increasing the ODT. Decreasing α caused the bottlebrush to behave more like a starblock copolymer, decreasing the ODT. Between these limits, the ODT changed monotonically. The periods, on the other hand, peaked at $\alpha \approx 0.35$, and decreased as the bottlebrush approached the diblock or starblock limits. Fluctuation corrections to the period in the ordered phase were particularly small. Despite having little effect on the ordered phase, fluctuations suppressed segregation, pushing the ODT to higher χN. This suggests a significant effect on the disordered phase, as has been seen in diblock copolymers.

The FTS are capable of handling bottlebrushes of various types. Furthermore, the simulations can be readily extended to consider the volume of the backbone and interactions with the grafts. In cases where the backbone is under high tension, it can easily be modeled as a freely-jointed chain with a finite extension. Reducing the invariant polymerization index is more challenging, but we are exploring ways of doing this.[45] The reason that this simulation method is so effective is that multiple identical grafts do not, in principle, increase the computational cost. In our case, the bottlebrush FTS was computationally equivalent

to that of a simple diblock copolymer. This approach should allow simulations of complex block copolymer architectures that would not be possible with conventional particle-based simulations.

Acknowledgments

We are grateful to Frank Bates and Michael Maher for valuable discussions. This work was funded through a collaboration with the University of Minnesota's Center for Sustainable Polymers (No. CHE-1413862). Calculations were performed using the SHARCNET facility of Compute Canada.

---

* Electronic address: r6spence@uwaterloo.ca

† Electronic address: mwmatsen@uwaterloo.ca

[1] Runge, M. B.; Bowden, N. B., *J. Am. Chem. Soc.* **129**, 10551 (2007).

[2] Runge, M. B.; Lipscomb, C. E.; Ditzler, L. R.; Mahanthappa, M. K.; Tivanski,A. V.; Bowden, N. B. *Macromolecules* **41**, 7687 (2008).

[3] Xia, Y.; Olsen, B. D.; Kornfield, J. A.; Grubbs, R. H. *J. Am. Chem. Soc.* **131**, 18525 (2009).

[4] Gerle, M.; Fischer, K.; Roos, S.; Müller, A.; *Macromolecules* **32**, 2629 (1999).

[5] Lecommandoux, S.; Chécot, F.; Borsali, R.; Schappacher, M.; Deffieux, A.; Brûlet, A.; Cotton, J. P. *Macromolecules* **35**, 8878 (2002).

[6] Sheiko, S. S.; Sumerlin, B. S.; Matyjaszewski, K. *Prog. Polym. Sci.* **33**, 759 (2008).

[7] Rzayev, J. *ACS Macro Lett.*, **1**, 1146 (2012).

[8] Verduzco, R.; Li, X.; Pesek, S. L.; Stein, G. E. *Chem. Soc. Rev.* **44**, 2405 (2005).

[9] Li, X.; Prukop, S. L.; Biswal, S. L.; Verduzco, R. *Macromolecules* **45**, 7118 (2012).

[10] Sveinbjörnsson, B. R.; Weitekamp, R. A.; Miyake, G. M.; Xia, Y.; Atwater, H. A.; Grubbs, P. H. *Proc. Natl. Acad. Sci. U.S.A.* **109**, 14332 (2012).

[11] Miyake, G. M.; Weitekamp, R. A.; Piunova, V. A.; Grubbs, R. H. *Macromolecules* **134**, 14249 (2012).

[12] Macfarlane, R. J.; Kim, B.; Lee, B.; Weitekamp, R. A.; Bates, C. M.; Lee, S. F.; Chang, A. B.; Delaney, K. T.; Fredrickson, G. H.; Atwater, H. A.; Grubbs, R. H. *J. Am. Chem. Soc.* **136**,

17374 (2014).

[13] Sun, G.; Cho, S.; Clark, C.; Verkhoturov, S. V.; Eller, M. J.; Li, A.; Pavía-Jiménez, A.; Schweikert, E. A.; Thackeray, J. W.; Trefonas, P.; Wooley, K. L. *J. Am. Chem. Soc.*, **135**, 4203 (2013).

[14] Zhang, J.; Li, T.; Mannion, A. M.; Schneiderman, D. K.; Hillmyer, M. A.; Bates, F. S. *ACS Macro Lett.* **5**, 407 (2016).

[15] Zhang, J.; Schneiderman, D. K.; Li, T.; Hillmyer, M. A.; Bates, F. S. *Macromolecules* **49**, 9108 (2016).

[16] Maher, M. J.; Jones, S. D.; Zografos, A.; Xu, J.; Schibur, H. J.; Bates, F. S. *Macromolecules* **51**, 232 (2018).

[17] Fredrickson, G. H. *Macromolecules* **26**, 2825 (1993).

[18] Cao, Z.; Carrillo, J.-M. Y.; Sheiko, S. S.; Dobrynin, A. V. *Macromolecules* **48**, 5006 (2015).

[19] Dalsin, S. J.; Rions-Maehren, T. G.; Beam, M. D.; Bates, F. S.; Hillmyer, M. A.; Matsen, M. W. *Macromolecules* **9**, 12233 (2015).

[20] Rzayev, J. *Macromolecules* **42**, 2135 (2009).

[21] Gu, W.; Huh, J.; Hong, S. W.; Sveinbjornsson, B. R.; Park, C.; Grubbs, R. H.; Russell, T. P. *ACS Nano* **7**, 2551 (2013).

[22] Chremos, A.; Theodorakis, P. E. *ACS Macro Lett.* **3**, 1096 (2014).

[23] Feuz, L.; Leermakers, F. A. M.; Textor, M.; Borisov, O. *Macromolecules* **38**, 8891 (2005).

[24] Düchs, D.; Delaney, K. T.; Fredrickson, G. H. *J. Chem. Phys.* **141**, 174103 (2014).

[25] Matsen, M. W. *Eur. Phys. J. E* **30**, 361 (2009).

[26] Düchs, D.; Ganesan, V.; Fredrickson, G. H.; Schmid, F. *Macromolecules* **36**, 9237 (2003).

[27] Stasiak, P.; Matsen, M. W. *Macromolecules* **46**, 8037 (2013).

[28] Stasiak, P.; Matsen, M. W. *Eur. Phys. J. E* **34**, 110 (2011).

[29] Fredrickson, G. H.; Helfand, E. *J. Chem. Phys.* **87**, 697 (1987).

[30] Vorselaars, B.; Stasiak, P.; Matsen, M. W. *Macromolecules* **48**, 9071 (2015).

[31] Spencer, R. K. W.; Matsen, M. W. *Macromolecules* **49**, 6116 (2016).

[32] de la Cruz, M. O.; Edwards, S. F.; Sanchez, I. C. *J. Chem. Phys.* **89**, 1704 (1988).

[33] Spencer, R. K. W.; Vorselaars, B.; Matsen, M. W. *Macromol. Theory Simul.* **26**, 1700036 (2017).

[34] Earl, D. J.; Deem, M. W. *Phys. Chem. Chem. Phys.* **7**, 3910 (2005).

[35] Lennon, E. M.; Katsov, K.; Fredrickson, G. H. *Phys. Rev. Lett.* **101**, 138302 (2008).

[36] Delaney, K. T.; Fredrickson, G. H. *J. Phys. Chem.* **120**, 7615 (2016).

[37] Leibler, L. *Macromolecules* **13**, 1602 (1980).

[38] Matsen, M.; Schick, M. *Phys. Rev. Lett.* **72**, 2660 (1994).

[39] Matsen, M. W. In *Soft Matter, Volume 1: Polymer Melts and Mixtures*; Gompper, G., Schick, M., Eds.; Wiley-VCH: Weinheim, 2006; pages 87–178.

[40] Olvera de la Cruz, M.; Sanchez, I. C. *Macromolecules* **19**, 2501 (1986).

[41] Matsen, M. W.; Schick, M. *Macromolecules* **27**, 6761 (1994).

[42] Glaser, J.; Medapuram, P.; Beardsley, T. M.; review, M. M. P.; *Phys. Rev. Lett.* **113**, 068302 (2014).

[43] Medapuram, P.; Glaser, J.; Morse, D. C. *Macromolecules* **48**, 819 (2015).

[44] Alexander-Katz, A; Fredrickson, G *Macromolecules* **40**, 4075 (2007).

[45] T. M. Beardsley, R. K. W. Spencer and M. W. Matsen, Manuscript in preparation.

[46] Glaser, J.; Qin, J.; Medapuram, P.; Morse, D. C. *Macromolecules* **47**, 851 (2014).

[47] Matsen, M. W. *Macromolecules* **45**, 8502 (2012).

[48] Fredrickson, G. H.; Ganesan, V.; Drolet, F. *Macromolecules* **35**, 16 (2002).

[49] Ganesan, V.; Fredrickson, G. H. *Europhys. Lett.* **55**, 814 (2007).

[50] Lennon, E. M.; Mohler, G. O.; Ceniceros, H. D.; García-Cervera, C. J.; Fredrickson, G. H. *Multiscale Model Sim.*, **6**, 1347 (2008).

[51] Qin, J.; Morse, D. C. *J. Chem. Phys.* **130**, 224902 (2009).

[52] Koski, J.; Chao, H.; Riggleman, R. A. *J. Chem. Phys.* **139**, 244911 (2013).